The remarkable surface homogeneity of the Dawn mission target (1) Ceres☆

Benoît Carry[a,b,c], Pierre Vernazza[d,e,f], Christophe Dumas[c], William J. Merline[g], Olivier Mousis[h], Philippe Rousselot[h], Emmanuël Jehin[i], Jean Manfroid[i], Marcello Fulchignoni[b], Jean-Marc Zucconi[h,1]

[a]*European Space Astronomy Centre, ESA, P.O. Box 78, 28691 Villanueva de la Cañada, Madrid, Spain*
[b]*LESIA, Observatoire de Paris-Meudon CNRS, 5 place Jules Janssen, 92195 Meudon Cedex, France*
[c]*European Southern Observatory, Alonso de Córdova 3107, Vitacura, Casilla 19001, Santiago de Chile, Chile*
[d]*European Southern Observatory, K. Schwarzschild-Str. 2, 85748 Garching, Germany*
[e]*Laboratoire dAstrophysique de Marseille, 38 rue Frédéric Joliot-Curie, 13388 Marseille, France*
[f]*Research and Scientific Support Department, ESA, Keplerlaan 1, 2201 AZ Noordwijk, The Netherlands*
[g]*Southwest Research Institute, 1050 Walnut St. # 300, Boulder, CO 80302, USA*
[h]*Université de Franche Comté - CNRS, Institut UTINAM, 41 bis av. de l'Observatoire, F-25010 Besançon Cedex, France*
[i]*Institut d'Astrophysique et de Géophysique, Université de Liège, B-4000 Liège, Belgium*

Abstract

Dwarf-planet (1) Ceres is one of the two targets, along with (4) Vesta, that will be studied by the NASA Dawn spacecraft via imaging, visible and near-infrared spectroscopy, and gamma-ray and neutron spectroscopy. While Ceres' visible and near-infrared disk-integrated spectra have been well characterized, little has been done about quantifying spectral variations over the surface. Any spectral variation would give us insights on the geographical variation of the composition and/or the surface age. The only work so far was that of Rivkin & Volquardsen (2010, Icarus 206, 327) who reported rotationally-resolved spectroscopic (disk-integrated) observations in the 2.2-4.0 μm range; their observations showed evidence for a relatively uniform surface.

Here, we report disk-resolved observations of Ceres with SINFONI (ESO VLT) in the 1.17-1.32 μm and 1.45-2.35 μm wavelength ranges. The observations were made under excellent seing conditions (0.6″), allowing us to reach a spatial resolution of ~75 km on Ceres' surface. We do not find any spectral variation above a 3% level, suggesting a homogeneous surface at our spatial resolution. Slight variations (about 2%) of the spectral slope are detected, geographically correlated with the albedo markings reported from the analysis of the HST and Keck disk-resolved images of Ceres (Li et al., 2006, Icarus 182, 143; Carry et al., 2008, A&A 478, 235). Given the lack of constraints on the surface composition of Ceres, however, we cannot assert the causes of these variations.

Keywords: ASTEROID CERES, SURFACES, ADAPTIVE OPTICS, INFRARED OBSERVATIONS

1. Introduction

Ceres, discovered in 1801 by Giuseppe Piazzi, is - with a diameter of 935 km (Carry et al. 2008) - by far the largest asteroid in the main asteroid belt. Interestingly, recent simulations (*e.g.*, Morbidelli et al. 2009, Minton and Malhotra 2009) have shown that in the early Solar System there must have been many Ceres-sized bodies to explain the current size-frequency distribution of asteroids. Ceres therefore appears to be a unique remnant of a dynamical removal process, which caused the Main Belt to lose most of its primordial mass. By furthering our understanding of the physical properties (*e.g.*, surface composition, density, internal structure) of the largest asteroids, we may be afforded a special opportunity to learn more about the formation process of large planetesimals from which terrestrial planets once accreted.

As one of the targets of the NASA Dawn mission (see Russell et al. 2004, for instance), Ceres recently has been the subject of increased attention from the community (*e.g.*, Parker et al. 2002, Nazzario et al. 2003, Thomas et al. 2005, Vernazza et al. 2005, McCord and Sotin 2005, Li et al. 2006, Rivkin et al. 2006, Chamberlain et al. 2007, Kovačević and Kuzmanoski 2007, Drummond and Christou 2008, Mousis et al. 2008, Milliken and Rivkin 2009, Chamberlain et al. 2009, Castillo-Rogez and McCord 2010, Moullet et al. 2010, Rousselot et al. 2011, and references therein). Three topics seem to have drawn the most attention: 1) characterization of the surface composition, 2) thermodynamic modeling of the interior, and 3) determination of the size, shape, spin, and albedo via disk-resolved imaging. We summarize the main results here:

1. While Ceres' exact surface composition remains elusive (see Rivkin et al. 2010, for a review), the analysis of the 2.9-4.0 μm region has allowed the possible detection of brucite and carbonate assemblages on its surface (Milliken and Rivkin 2009), suggesting that the thermal and aqueous alteration history of Ceres differs from that in the record of carbonaceous meteorites.
2. Modeling of Ceres' thermo-physical-chemical evolution

☆Based on observations collected at the European Organisation for Astronomical Research in the Southern Hemisphere, Chile - program ID: 080.C-0881.

[1]Deceased

has pointed to a differentiated interior for Ceres, in accord with shape measurements (Thomas et al. 2005, Carry et al. 2008). The interior would consist of an inner core of dry silicates, an intermediate layer of hydrated silicates, and an outer shell of water ice (Castillo-Rogez and McCord 2010). However, an undifferentiated Ceres consisting of a homogeneous mixture of hydrated silicates is still possible (Zolotov 2009).

3. Disk-resolved imaging of Ceres has allowed determination of its size, shape, and spin with small uncertainties, in turn constraining the density (Thomas et al. 2005, Carry et al. 2008). Finally, the images showed surface albedo variations of 6 % around the average surface value, with putative, broad-band, color variations (≈2–3%, see Li et al. 2006, Carry et al. 2008). The cause of the color contrast (*e.g.*, geological features, composition, grain properties, surface age) could not be determined.

While Ceres' visible and near-infrared spectrum has been well characterized, little has been done about quantifying spectral variations over the surface. Disk-resolved analysis would give us insights on the geographical variation of the composition and/or variation in ages of surface units. The only disk-resolved analyses done so far were those of Parker et al. (2002), Li et al. (2006), and Carry et al. (2008), studying the albedo/color variations in the visible and near-infrared only. Observations at other wavelegths were limited to disk-integrated observations and could only search for rotational modulation of the spectra. All studies showed evidence for a relatively uniform surface. A summary of the disk-integrated results is given here:

1. Polarization: no rotational variation reported at visible wavelengths (Rivkin et al. 2010), although a slight variation of 0.1% in the degree of polarization can be surmised from the literature (I. Belskaya, personnal communication)
2. Visible photometry: low-amplitude lightcurve due to albedo features (Tedesco et al. 1983).
3. Near-infrared spectroscopy: marginal ($1\,\sigma$) variations of brucite- and carbonates-associated absorption bands (Rivkin and Volquardsen 2010), indicating a homogeneous mineralogy with tenuous evidence for variations.
4. Far infrared radiometry: very low-amplitude lightcurve (Altenhoff et al. 1996, Moullet et al. 2010), indicating an overall homogeneous surface and subsurface properties (roughness, absorption coefficient, refractive index, and thermal inertia).

Although the disk-integrated spectrum of Ceres presents more absorption features in the 2.9-4.0 μm region (*e.g.*, Rivkin et al. 2010, and references therein), we report an analysis of ground-based disk-resolved spectral observations of Ceres' surface in the near-infrared (1.1-2.4 μm) to investigate with better spectral resolution the surface features detected by Carry et al. (2008) from disk-resolved, broad-band, imaging observations. At this time, high-angular-resolution imaging spectrographs can only operate in the near-infrared range. In Section 2 we describe the observations and the data reduction, in Section 3 we present the spectral analysis, and in Section 4 we discuss the spectral heterogeneity across Ceres' surface.

2. Observations and Data Reduction

We made disk-resolved observations of (1) Ceres on 2007 November 13, covering about 2/3 of its 9.074 h rotation (Chamberlain et al. 2007, Carry et al. 2008). The observations were made in the near-infrared with the integral-field spectrograph SINFONI (using the J: 1.17-1.32 μm and H+K: 1.45-2.35 μm gratings, with a resolving power of 2000 and 1500 respectively, see Eisenhauer et al. 2003, Bonnet et al. 2004) at the European Southern Observatory (Cerro Paranal, Chile) with one (UT4/Yepun) of the four 8-m telescopes of the Very Large Telescope (VLT) facility.

Atmospheric conditions were excellent, with a seeing at visible wavelengths of about 0.6″ (reaching 1.1″ at worst) and a coherence time of 2–4 ms. The adaptive optics module of SINFONI was providing a high-quality correction: the wavefront sensor used Ceres itself (V ~ 7.3) as a reference, allowing high-frequency correction (420 Hz). Identical settings were used for the observation of the standard stars (see below), and the quality of the correction was similar in both cases.

The apparent diameter of Ceres at the time of the observation was about 0.7″, so to search for spectral variations across the asteroid surface, we used the high-angular-resolution mode with an equivalent pixel size on sky of 25×12.5 milli-arcsec and a field of view of 0.8×0.8 arcsecond. The high angular resolution, resulting from the adaptive-optics correction coupled with the excellent seeing conditions we had throughout the night (see Table 1), allowed us to reach an average spatial resolution on Ceres' surface of about 75 km (ranging from 55 to 98 km, depending on the wavelength, see Table 2). The same jitter pattern was used at all epochs to ensure complete coverage of Ceres' apparent disk given the narrow field of view: a single exposure of Ceres is made at the center of the pattern, followed by four others, taken in (x,y) steps of ± 0.2 arcsec from the central position. Then three sky exposures are taken 30″ away from Ceres (East - North - West). Exposure times were 90 s and 40 s in J and H+K, respectively (we used 4 s and 1 s, respectively, for the standard stars).

The observing circumstances are reported in Table 1. We list the mid-observation time (UT), grating used (J or H+K), longitude of the sub-Earth and subsolar points (SEP_λ and SSP_λ, respectively, computed using the pole solution by Carry et al. (2008)), airmass (X), and seeing (*s*). During our observations, the latitude of the SEP and SSP was constant, of 3° and 0°, respectively.

Observations of standard (PSF) stars were interspersed with Ceres observations throughout the night. Two stars were used: HD 15474 (G5) and HD 28099 (G2V). Both stars have V ~ 8.1, slightly dimmer than Ceres (V ~ 7.3 at the time of the observations), and were located at 8.5° and 22° from Ceres respectively. We list in Table 2 the circumstances for those observations, namely the mid-observation time (UT), the grating used (J or H+K), the airmass (X), and the angular resolution measured on the star itself after data reduction (Θ, corresponding

Time (UT)	Grating	SEP_λ (°)	SSP_λ °)	X	s (″)
00:48	H+K	211	213	2.04	0.79
00:58	H+K	204	206	1.92	0.67
01:12	J	195	197	1.77	1.28
01:55	H+K	167	169	1.49	0.73
02:05	H+K	160	162	1.44	1.10
02:20	J	150	152	1.37	1.09
02:57	H+K	125	127	1.27	0.61
03:07	H+K	119	121	1.25	0.57
03:18	J	111	113	1.23	0.61
03:57	H+K	86	88	1.19	1.10
04:07	H+K	79	81	1.19	1.11
04:18	J	72	74	1.19	1.10
04:37	H+K	60	62	1.19	1.04
04:46	H+K	53	55	1.20	n.a.
04:58	J	46	47	1.21	0.86
05:16	H+K	34	36	1.23	0.72
05:26	H+K	27	29	1.25	0.78
05:37	J	20	22	1.27	0.62
06:15	H+K	355	356	1.38	0.75
06:25	H+K	348	350	1.42	0.60
06:36	J	341	343	1.47	0.56
07:10	H+K	318	320	1.68	0.45

Table 1: Observing circumstances for (1) Ceres. For each observation, we report the mid-observation time in UT, the grating used to disperse the light, the longitude (λ) of the sub-Earth point (SEP) and subsolar point (SSP), their respective latitude β being 3° and 0°, the airmass (X), and the seeing (s).

Time (UT)	Grating	X	s (″)	Θ_J (″)	Θ_H (″)	Θ_K (″)
00:34	J	1.82	0.72	0.030	–	–
01:44	J	1.39	1.33	0.042	–	–
02:47	J	1.23	0.75	0.045	–	–
03:47	J	1.19	n.a.	0.042	–	–
06:05†	J	1.34	0.58	0.047	–	–
07:02	J	1.92	0.53	0.043	–	–
00:23	H+K	1.92	0.64	–	0.049	0.076
01:36	H+K	1.42	1.24	–	0.054	0.069
02:41	H+K	1.24	0.73	–	0.052	0.070
03:41	H+K	1.19	n.a.	–	0.057	0.068
05:58†	H+K	1.34	0.54	–	0.054	0.080
06:56	H+K	1.87	0.55	–	0.053	0.076
		Average		0.041	0.052	0.073
		Theoretical		0.031	0.041	0.057
		Deviation		0.006	0.003	0.005

Table 2: Observing circumstances for standard stars. For each observation, we report the mid-observation time in UT, the airmass (X), the seeing (s), and the size of the resolution element, measured as the FWHM of the stars (Θ), for each band: J, H, and K (*i.e.*, at 1.22, 1.60, and 2.2 μm). The theoretical angular resolution (defined here as the diffraction limit λ/D, with λ the wavelength and D the telescope aperture) is also reported. The average FWHMs of the PSFs correspond to spatial resolutions of 55, 71, and 98 km respectively (projected to the distance of Ceres). The observation marked with a dagger (†) corresponds to the single observation of HD 28099.

to its full width at half maximum, FWHM). Although the seeing and airmass varied thorough the night, the angular resolution provided by the AO correction was very stable (Table 2). We therefore consider that the spatial resolution at Ceres was 55, 71, and 98 km in the J, H, and K-band wavelength ranges (the resolution decreasing continuously from the shortest wavelength to the longest).

The basic data reduction was performed using the ESO pipeline 2.0.5 (Modigliani et al. 2007): 1) correction of the object-sky pairs for bad pixels and flat-field effects, 2) wavelength calibration, 3) sky subtraction, and 4) reconstruction of the final image cubes (the 3-dimensional "cubes" consist of many 2-dimensional images of Ceres; the third dimension is wavelength, with one image for each wavelength channel). As already discussed by Carry et al. (2010), the grazing viewing angle near Ceres' limb causes unreliable flux measurement for the outer annulus of the asteroid's apparent disk. Therefore, we restricted our study to a "region of interest" (ROI), covering the innermost portion of the apparent disk. The ROI was defined to be the central region of the disk, within 75% of Ceres' radius, (following Carry et al. 2008).

Each spectrum extracted within the ROI was divided by the spectrum of a standard star, taken close in time and in airmass (see Table 1 and Table 2), to ensure the best possible correction for atmospheric effects, particularly water vapor. Remaining bad pixels and cosmic rays were removed by applying a median filter to the reflectance spectra. The box size was set to 5 pixels, corresponding to 0.7 and 2.5 nm for J and H+K gratings respectively. This width is narrow enough to have no influence on the detection of absorption bands (resolving power remains of several hundreds. The spectra are normalized to unity at 1.17 μm and 1.50 μm, respectively. These reflectance spectra are plotted for each epoch in Figs 1 and 2.

3. Spectral analysis

Our observations covered most of Ceres's low-latitude regions (see Table 1, and Fig. 3). In both wavelength ranges, we observe very little deviation from the average (see Figs 1 and 2). To quantify precisely how the different reflectance spectra behave with respect to the average, we utilized the two following norms, sensitive to spectral deviation (*i.e.*, presence of absorption band), that we applied to all the spectra of each image-cube (both J and H+K; spectra within the ROI) before (case *a*) and after (case *b*) division by their spectral slope (≈continuum, renormalized to unity at 1.17 μm and 1.50 μm, see Sect. 2):

$$\sigma_i = \frac{\sum_\lambda (\mathcal{S}_i - 1)}{\sum_\lambda (\mathcal{S}^\star - 1)} \quad (1)$$

$$\chi^2_i = \frac{\sum_\lambda (\mathcal{S}_i - 1)^2}{\sum_\lambda (\mathcal{S}^\star - 1)^2} \quad (2)$$

where σ_i and χ^2_i are the reduced "*deviation*" and "*chi-square*" norms, $\mathcal{S}^\star$ the slope-removed spectrum used to estimate the

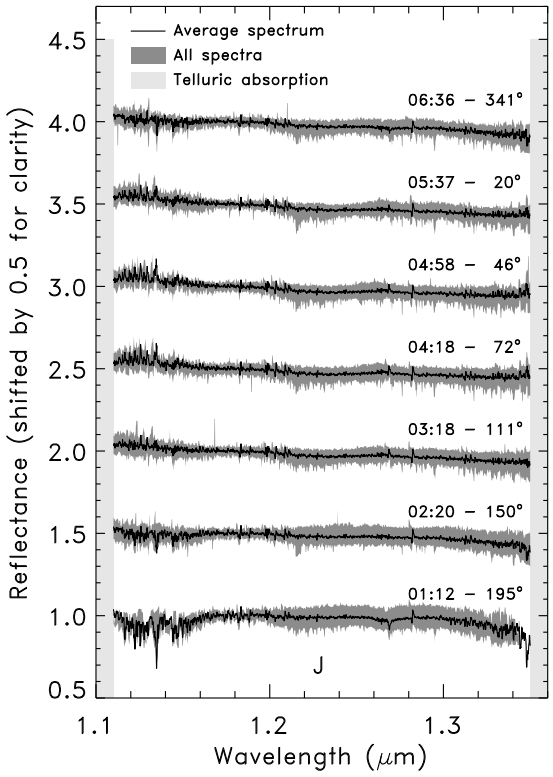

Figure 1: Reflectance spectra obtained with the J grating. For each epoch, the average spectrum (black line) and all the individual spectra within the ROI (dark-gray area) are plotted. The wavelength ranges affected by telluric absorptions (*i.e.*, the limits of the J-band) are displayed in light gray and the spectra are omitted for clarity. The mid-observation time (UT time on 2007 Nov 13) and the longitude of the sub-Earth point (SEP$_\lambda$, see Table 1) are reported for each epoch.

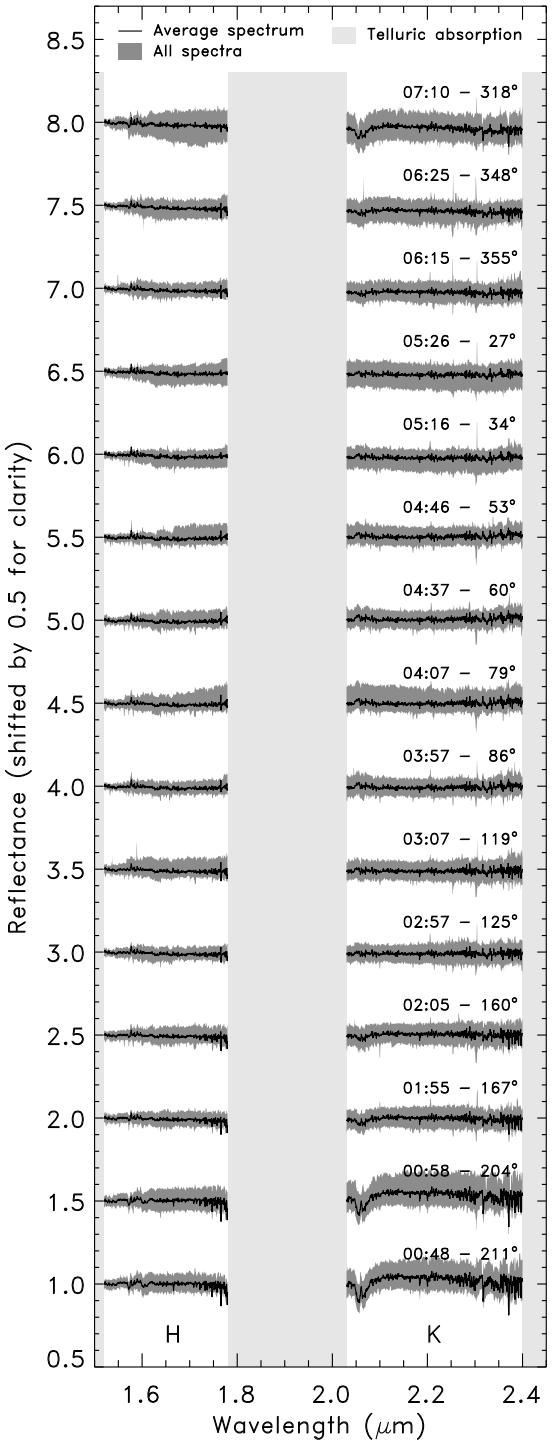

Figure 2: Reflectance spectra obtained with the H+K grating. For each epoch, the average spectrum (black line) and all the individual spectra with the ROI (dark-gray area) are plotted. The wavelength ranges affected by telluric absorptions (*i.e.*, the limits of the H- and K-bands) are displayed as the light gray area and the spectra are omitted for clarity. The mid-observation time (UT time on 2007 Nov 13) and the longitude of the sub-Earth point (SEP$_\lambda$, see Table 1) are reported for each epoch. Absorption features at 2.05 μm visible in spectra taken at 00:48, 00:58, and 07:10 are telluric absorption not fully-corrected due to the high airmass of Ceres during the observations.

noise, $\mathcal{S}_i$ the spectrum normalized by the disk-integrated average spectrum (all the spectra within the ROI); the subscript i standing for cases a and b.

Because both norms are reduced (*i.e.*, they are normalized by a measure of the noise), they give the level of confidence at which a variation from the disk-integrated average spectrum is detected: a spectrum equal to the average spectrum at all wavelengths has a norm of 0, and a spectrum whose deviations to the average spectrum are smaller than its intrinsic noise will have a norm below 1.

We applied the norms before (a) and after (b) slope removal to test if the spectral variation was mainly a slope variation or if it could also be due to the presence of absorption bands.

We display in Fig. 4 the distribution of these two norms, computed for the 10 619 and 22 755 individual spectra obtained with the J and H+K gratings respectively. First, both distributions are sharper, and mostly below 1, after slope removal (case b) than before (case a). This computation highlights the small spectral variation, mostly due to slope variation, of each spectrum with respect to the average one.

We then focused our attention on spectra with χ^2_b norm above 1, to check whether the variation is real or due to an instrumental artifact, and if real whether the variation is due to the repeated presence of an absorption band. Reflectance spectra with higher norms appeared at fixed positions on the SINFONI

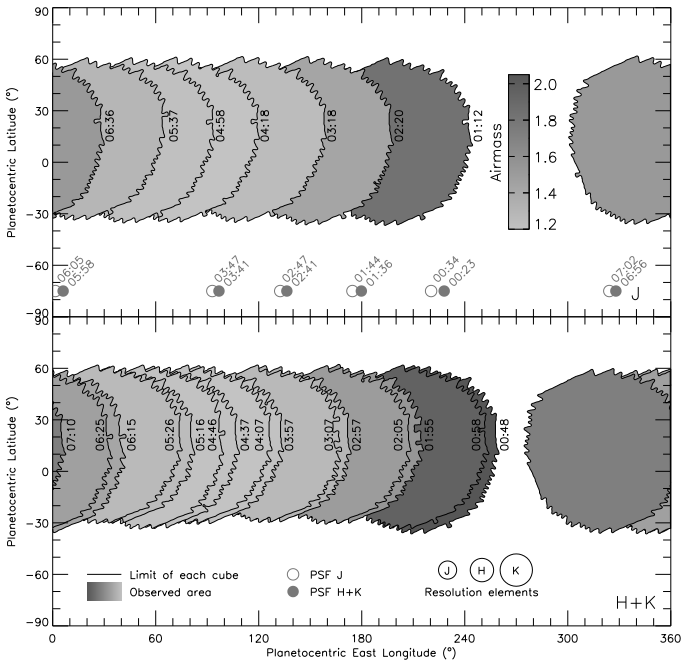

Figure 3: Equidistant cylindrical projections showing the coverage of our observations (ROI only) on Ceres' surface. Each image cube is delimited by a black contour and shaded as a function of airmass at the time of the observation (Table 1). The observing time of each image cube is reported near its eastern border. *Top*: the 7 image cubes using the J grating. Filled and empty circles (arbitrary size), labeled with UT times, indicate the rotational phase of Ceres at the observation time of the standard stars with the H+K and J grating, respectively. *Bottom*: the 15 image cubes using the H+K grating. The size of the resolution elements at each wavelength range (55, 71, and 98 km at J, H, and K-band) are represented here, as if projected on Ceres equator.

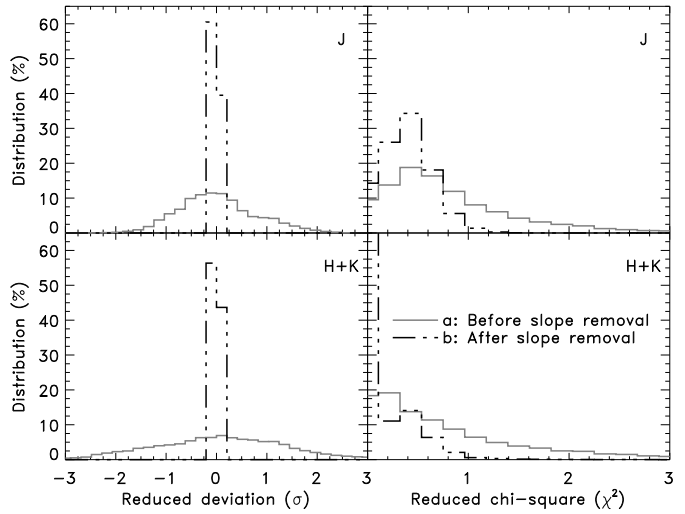

Figure 4: Reduced deviation (σ, left) and chi-square (χ^2, right) norms distribution for both J (top) and H+K (bottom) spectra, before (case *a*, gray histogram) and after (case *b*, black histogram) slope removal.

detector, instead of following the rotation of Ceres. We thus conclude on the absence of absorption band in J, H and K-band wavelengths at our noise level (1-σ): 3.7% in J, 1.4% in H, and 1.8% in K. Considering the depth of the characteristics absorption bands of water ice, centered at 1.6 and 2.2 μm, this sets an upper limit of approximately 1% for ice frost geometric coverage.

We finally investigated the spatial distribution of the spectral slope variation. For each spatial pixel, we computed the spectral slope, and mapped it onto an Equidistant Cylindrical Projection (ECP) (Fig 5), following Carry et al. (2010). The slope variations were reproduced from image cube to image cube, and were thus linked to the instrument. We corrected this cosmetic problem by subtracting an average slope map at each image cube. The first observations of the night were more affected by this noise pattern, and some residuals are still present in the slope maps presented in Fig. 5, between 120° and 240° East in J, and between 180° and 250° East in H+K (corresponding to high-airmass observations, see Fig. 3 and Table 1). The slope information at these location is not reliable, and interpretations must be cautious.

No slope variations are detected in the J-band wavelength range, all the deviations to the average spectral slope (neutral between 1.10 and 1.35 μm) appearing suspicious. We, however, detect possible genuine variations (slope only) over the H+K wavelength range in five regions, labeled A to E (Fig. 5). Three of them (B, C, and E) present a lower spectral slope (about 2%/μm) than the surroundings (the average spectral slope of Ceres in that wavelength range is of about 4%/μm). These location are associated with low-albedo markings at visible and near-infrared wavelengths: feature #7, central part of #2, and East of #6 in Fig. 5 by Li et al. (2006) and features d_1 and d_3 in Fig. 7 by Carry et al. (2008). The other two features (A and D) have higher spectral slopes (above 5%/μm) and are associated with high albedo markings: features #1 and #5 in Fig. 5 by Li et al. (2006) and feature b_4 in Fig. 7 by Carry et al. (2008).

Feature D is one of the highest slopes measured in the J-band map, although it falls on one of the main noise residuals. It corresponds to the dark feature with a central bright peak seen in the near-infrared images (Carry et al. 2008). If this round-shaped feature is associated with an impact crater, the observed differences in reflectivity and spectral slope may be related to differences in surface age ("fresher" material excavated), or regolith properties (different packing). Given the relative lack of constrains on the surface composition of Ceres, we cannot assert the causes of these variations. We only report here on the detection of spectral slope variations correlated to albedo markings.

4. Discussion

The handful of features detected here contrasts with the wealth of albedo markings reported by Li et al. (2006) and Carry et al. (2008) based on broad-band photometry in the visible and near-infrared with HST/ACS and Keck/NIRC2, respectively. However, both analyses used deconvolution techniques, which enhance the spatial resolution and photometric contrast. The data presented here still suffers from aberrations introduced by the not fully-corrected atmospheric turbulence, and non-perfect optics of the instrument and telescope. The encircled energy within a resolution element (the core of the PSF, corresponding

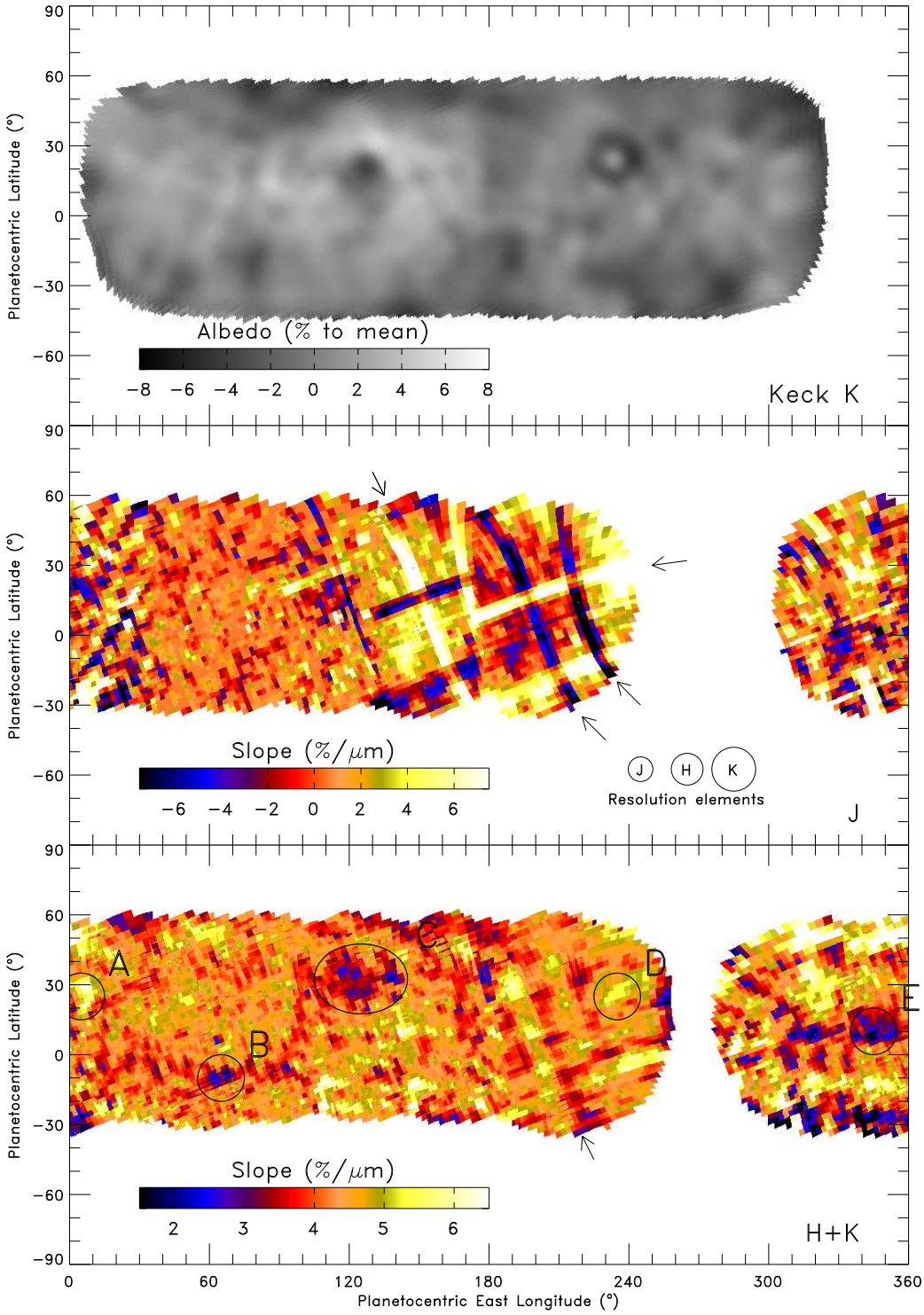

Figure 5: Equidistant Cylindrical Projection maps of the spectral slope measured in J (middle) and H+K (bottom) wavelength ranges, compared with the K-band albedo map (top) from Carry et al. (2008). The size of the resolution elements at each wavelength range (55, 71, and 98 km at J, H, and K-band) are represented here (middle map), as if projected on Ceres' equator. No features above the noise level are reliably seen in the J-band map, and most of the small-scale features seen in H+K are likely noise. There are five regions where the slope deviates from the average (about 4%/μm in H+K), labeled from A to E on the H+K map. The main uncorrected noise patterns (stripes crossing the field of view) are highlighted with arrows (see text).

to about 75 km on the surface of Ceres) will thus only be a portion of the total energy.

The information is thus spread out and averaged with nearest-neighbor pixels, lowering the photometric contrast (albedo vari-

ations are barely distinguishable on non-deconvolved images of Ceres used by Carry et al. 2008, although being perfectly distinguishable after deconvolution). This highlights the need for deconvolution algorithms for spectro-imaging.

Nevertheless, the apparent homogeneity of the surface composition of Ceres might be consistent with the hypothesis of a differentiated interior. McCord and Sotin (2005) have suggested that a thin ice-silicate crust would be probably unstable if it overlays a less dense liquid-water layer. In this case, the crust would tend to break up and founder probably soon after the liquid-water mantle formed in the first tens of Myr after formation. A new crust would then quickly freeze out and thus resurface Ceres by mixing and/or depositing minerals on the surface, erasing major albedo and morphological features (Li et al. 2006, Carry et al. 2008). If this mixing was efficient, then the surface of Ceres may have acquired a homogeneous composition at early epochs of its evolution. Alternatively, this homogeneity could be also explained by resurfacing processes induced by (ancient or more recent) cryovolcanism (Castillo-Rogez and McCord 2010). In both scenarios, the short sublimation timescale of the ice brought to the surface of the asteroid makes its detection unlikely.

5. Conclusion

We present the first disk-resolved spectroscopic observations of dwarf-planet (1) Ceres in the near-infrared (1.1–2.4 μm). Our observations used SINFONI on the ESO Very Large Telescope and had an angular resolution of about 0.040″, corresponding to ∼75 km on the surface of Ceres, and a spectral resolving power of about 1500.

We did not detect any absorption band at the 3.0%, 1.2%, and 1.3% levels in J, H and K bands, respectively. Variations of the spectral slope are observed over the surface, with dark and bright albedo markings (few percent variations detected from visible and near-infrared imaging, see Li et al. 2006, Carry et al. 2008) presenting respectively a lower and higher spectral slope (couple of percent per micron) than the surroundings. The surface of Ceres is thus remarkably homogeneous at our spatial and spectral resolutions.

Acknowledgments

This research used IMCCE's Miriade VO tool and NASA's Astrophysics Data System. A great thanks to all the developers and maintainers. BC and PV thank the ESA Visiting Scientist Program. EJ and JM are Research Associate and Research Director of the FRS-FNRS, Belgium. We thank both anonymous referees for their valuable comments that helped us in improving this manuscript.

References

W. J. Altenhoff, J. W. M. Baars, J. B. Schraml, P. Stumpff, and A. von Kap-Herr, 1996. Precise flux density determination of 1 Ceres with the Heinrich-Hertz-Telescope at 250Hz. Astronomy and Astrophysics, 309:953–956.

H. Bonnet, R. Abuter, A. Baker, W. Bornemann, A. Brown, R. Castillo, R. D. Conzelmann, R. Damster, R. Davies, B. Delabre, R. Donaldson, C. Dumas, F. Eisenhauer, E. Elswijk, E. Fedrigo, G. Finger, H. Gemperlein, R. Genzel, A. Gilbert, G. Gillet, A. Goldbrunner, M. Horrobin, R. Ter Horst, S. Huber, N. N. Hubin, C. Iserlohe, A. Kaufer, M. Kissler-Patig, J. Kragt, G. Kroes, M. D. Lehnert, W. Lieb, J. Liske, J.-L. Lizon, D. Lutz, A. Modigliani, G. J. Monnet, N. Nesvadba, J. Patig, J. Pragt, J. Reunanen, C. Röhrle, S. Rossi, R. Schmutzer, T. Schoenmaker, J. Schreiber, S. Stroebele, T. Szeifert, L. Tacconi, M. Tecza, N. A. Thatte, S. Tordo, P. van der Werf, and H. Weisz, 2004. First light of SINFONI at the VLT. The Messenger, 117:17–24.

B. Carry, C. Dumas, M. Fulchignoni, W. J. Merline, J. Berthier, D. Hestroffer, T. Fusco, and P. Tamblyn, 2008. Near-Infrared Mapping and Physical Properties of the Dwarf-Planet Ceres. Astronomy and Astrophysics, 478(4): 235–244.

B. Carry, P. Vernazza, C. Dumas, and M. Fulchignoni, 2010. First disk-resolved spectroscopy of (4) Vesta. Icarus, 205:473–482.

J. C. Castillo-Rogez and T. B. McCord, 2010. Ceres: evolution and present state constrained by shape data. Icarus, 205:443–459.

M. A. Chamberlain, A. J. Lovell, and M. V. Sykes, 2009. Submillimeter photometry and lightcurves of Ceres and other large asteroids. Icarus, 202: 487–501.

M. A. Chamberlain, M. V. Sykes, and G. A. Esquerdo, 2007. Ceres lightcurve analysisPeriod determination. Icarus, 188(2):451–456.

J. D. Drummond and J. C. Christou, 2008. Triaxial ellipsoid dimensions and rotational poles of seven asteroids from Lick Observatory adaptive optics images, and of Ceres. Icarus, 197:480–496.

F. Eisenhauer, R. Abuter, K. Bickert, F. Biancat-Marchet, H. Bonnet, J. Brynnel, R. D. Conzelmann, B. Delabre, R. Donaldson, J. Farinato, E. Fedrigo, R. Genzel, N. N. Hubin, C. Iserlohe, M. E. Kasper, M. Kissler-Patig, G. J. Monnet, C. Roehrle, J. Schreiber, S. Stroebele, M. Tecza, N. A. Thatte, and H. Weisz, 2003. SINFONI - Integral field spectroscopy at 50 milli-arcsecond resolution with the ESO VLT. SPIE, 4841:1548–1561.

A. Kovačević and M. Kuzmanoski, 2007. A New Determination of the Mass of (1) Ceres. Earth Moon and Planets, 100:117–123.

J.-Y. Li, L. A. McFadden, J. W. Parker, E. F. Young, S. A. Stern, P. C. Thomas, C. T. Russell, and M. V. Sykes, 2006. Photometric analysis of 1 Ceres and surface mapping from HST observations. Icarus, 182:143–160.

T. B. McCord and C. Sotin, 2005. Ceres: Evolution and current state. Journal of Geophysical Research (Planets), 110:5009–5023.

R. E. Milliken and A. S. Rivkin, 2009. Brucite and carbonate assemblages from altered olivine-rich materials on Ceres. Nature Geoscience, 2:258–261.

D. A. Minton and R. Malhotra, 2009. A record of planet migration in the main asteroid belt. Nature, 457:1109–1111.

A. Modigliani, W. Hummel, R. Abuter, P. Amico, P. Balleste, R. Davies, C. Dumas, M. Horrobin, M. Neeser, M. Kissler-Patig, M. Peron, J. Rehunanen, J. Schreiber, and T. Szeifert, 2007. The SINFONI pipeline. ArXiv Astrophysics e-prints.

A. Morbidelli, W. F. Bottke, D. Nesvorný, and H. F. Levison, 2009. Asteroids were born big. Icarus, 204:558–573.

A. Moullet, M. Gurwell, and B. Carry, 2010. Thermal rotational lightcurve of dwarf-planet (1) Ceres at 235 GHz with the Submillimeter Array. Astronomy and Astrophysics, 516:L10.

O. Mousis, Y. Alibert, D. Hestroffer, U. Marboeuf, C. Dumas, B. Carry, J. Horner, and F. Selsis, 2008. Origin of volatiles in the main belt. Monthly Notices of the Royal Astronomical Society, 383:1269–1280.

R. Nazzario, T. W. Hyde, and L. Barge, 2003. Dust grain orbital behavior around ceres. Advances in Space Research, 31:2591–2597.

J. W. Parker, S. A. Stern, P. C. Thomas, M. C. Festou, W. J. Merline, E. F. Young, R. P. Binzel, and L. A. Lebofsky, 2002. Analysis of the First Disk-resolved Images of Ceres from Ultraviolet Observations with the Hubble Space Telescope. The Astronomical Journal, 123:549–557.

A. S. Rivkin, J.-Y. Li, R. E. Milliken, L. F. Lim, A. J. Lovell, B. E. Schmidt, L. A. McFadden, and B. A. Cohen, 2010. The Surface Composition of Ceres. Space Science Reviews, page 101.

A. S. Rivkin and E. L. Volquardsen, 2010. Rotationally-resolved spectra of Ceres in the 3-μm region. Icarus, 206:327–333.

A. S. Rivkin, E. L. Volquardsen, and B. E. Clark, 2006. The surface composition of Ceres: Discovery of carbonates and iron-rich clays. Icarus, 185: 563–567.

P. Rousselot, O. Mousis, C. Dumas, E. Jehin, J. Manfroid, B. Carry, and J.-M. Zucconi, 2011. A search for water vaporization on Ceres. submitted to AJ,

1405:8337.

C. T. Russell, A. Coradini, U. Christensen, M. C. De Sanctis, W. C. Feldman, R. Jaumann, H. U. Keller, A. S. Konopliv, T. B. McCord, L. A. McFadden, H. Y. McSween Jr., S. Mottola, G. Neukum, C. M. Pieters, T. H. Prettyman, C. A. Raymond, D. E. Smith, M. V. Sykes, B. G. Williams, J. Wise, and M. T. Zuber, 2004. Dawn: A journey in space and time. Planetary and Space Science, 52:465–489.

E. F. Tedesco, R. C. Taylor, J. D. Drummond, D. Harwood, I. Nickoloff, F. Scaltriti, H. J. Schober, and V. Zappala, 1983. Worldwide photometry and lightcurve observations of 1 Ceres during the 1975-1976 apparition. Icarus, 54:23–29.

P. C. Thomas, J. W. Parker, L. A. McFadden, C. T. Russell, S. A. Stern, M. V. Sykes, and E. F. Young, 2005. Differentiation of the asteroid Ceres as revealed by its shape. Nature, 437:224–226.

P. Vernazza, T. Mothé-Diniz, M. A. Barucci, M. Birlan, J. M. Carvano, G. Strazzulla, M. Fulchignoni, and A. Migliorini, 2005. Analysis of near-IR spectra of 1 Ceres and 4 Vesta, targets of the Dawn mission. Astronomy and Astrophysics, 436:1113–1121.

M. Y. Zolotov, 2009. On the composition and differentiation of Ceres. Icarus, 204:183–193.